Metallic artifacts from internal scaphoid fracture fixation screws: Comparison between C-Arm flat-panel, cone-beam, and multidetector computed tomography

Finkenstaedt, Tim ; Morsbach, Fabian ; Calcagni, Maurizio ; Vich, Magdalena ; Pfirrmann, Christian W A ; Alkadhi, Hatem ; Runge, Val M ; Andreisek, Gustav ; Guggenberger, Roman

Abstract: OBJECTIVES: The aim of this study was to compare image quality and extent of artifacts from scaphoid fracture fixation screws using different computed tomography (CT) modalities and radiation dose protocols. MATERIALS AND METHODS: Imaging of 6 cadaveric wrists with artificial scaphoid fractures and different fixation screws was performed in 2 screw positions (45° and 90° orientation in relation to the x/y-axis) using multidetector CT (MDCT) and 2 flat-panel CT modalities, C-arm flat-panel CT (FPCT) and cone-beam CT (CBCT), the latter 2 with low and standard radiation dose protocols. Mean cartilage attenuation and metal artifact-induced absolute Hounsfield unit changes (= artifact extent) were measured. Two independent radiologists evaluated different image quality criteria using a 5-point Likert-scale. Interreader agreements (Cohen) were calculated. Mean absolute Hounsfield unit changes and quality ratings were compared using Friedman and Wilcoxon signed-rank tests. RESULTS: Artifact extent was significantly smaller for MDCT and standard-dose FPCT compared with CBCT low- and standard-dose acquisitions (all $P < 0.05$). No significant differences in artifact extent among different screw types and scanning positions were noted ($P > 0.05$). Both MDCT and FPCT standard-dose protocols showed equal ratings for screw bone interface, fracture line, and trabecular bone evaluation ($P = 0.06$, 0.2, and 0.2, respectively) and performed significantly better than FPCT low- and CBCT low- and standard-dose acquisitions (all $P < 0.05$). Good interreader agreement was found for image quality comparisons (Cohen = 0.76-0.78). CONCLUSIONS: Both MDCT and FPCT standard-dose acquisition showed comparatively less metal-induced artifacts and better overall image quality compared with FPCT low-dose and both CBCT acquisitions. Flat-panel CT may provide sufficient image quality to serve as a versatile CT alternative for postoperative imaging of internally fixated wrist fractures.

DOI: https://doi.org/10.1097/RLI.0000000000000052

Metallic Artifacts From Internal Scaphoid Fracture Fixation Screws

Comparison Between C-Arm Flat-Panel, Cone-Beam, and Multidetector Computed Tomography

Tim Finkenstaedt, MD, Fabian Morsbach, MD,* Maurizio Calcagni, MD,† Magdalena Vich, MD,‡ Christian W.A. Pfirrmann, MD, MBA,§ Hatem Alkadhi, MD, MPH, EBCR,* Val M. Runge, MD,* Gustav Andreisek, MD, MBA,* and Roman Guggenberger, MD**

Objectives: The aim of this study was to compare image quality and extent of artifacts from scaphoid fracture fixation screws using different computed tomography (CT) modalities and radiation dose protocols.

Materials and Methods: Imaging of 6 cadaveric wrists with artificial scaphoid fractures and different fixation screws was performed in 2 screw positions (45° and 90° orientation in relation to the x/y-axis) using multidetector CT (MDCT) and 2 flat-panel CT modalities, C-arm flat-panel CT (FPCT) and cone-beam CT (CBCT), the latter 2 with low and standard radiation dose protocols. Mean cartilage attenuation and metal artifact–induced absolute Hounsfield unit changes (= artifact extent) were measured. Two independent radiologists evaluated different image quality criteria using a 5-point Likert-scale. Interreader agreements (Cohen κ) were calculated. Mean absolute Hounsfield unit changes and quality ratings were compared using Friedman and Wilcoxon signed-rank tests.

Results: Artifact extent was significantly smaller for MDCT and standard-dose FPCT compared with CBCT low- and standard-dose acquisitions (all $P < 0.05$). No significant differences in artifact extent among different screw types and scanning positions were noted ($P > 0.05$). Both MDCT and FPCT standard-dose protocols showed equal ratings for screw bone interface, fracture line, and trabecular bone evaluation ($P = 0.06$, 0.2, and 0.2, respectively) and performed significantly better than FPCT low- and CBCT low- and standard-dose acquisitions (all $P < 0.05$). Good interreader agreement was found for image quality comparisons (Cohen $\kappa = 0.76$–0.78).

Conclusions: Both MDCT and FPCT standard-dose acquisition showed comparatively less metal-induced artifacts and better overall image quality compared with FPCT low-dose and both CBCT acquisitions. Flat-panel CT may provide sufficient image quality to serve as a versatile CT alternative for postoperative imaging of internally fixated wrist fractures.

Key Words: computed tomography, flat panel, cone beam, metal artifacts, image quality

(*Invest Radiol* 2014;49: 532–539)

Internal fixation screws are used to enhance primary bone healing in scaphoid fractures and to reduce fracture-associated complications such as pseudoarthrosis and osteonecrosis.[1,2] However, postoperative complications may arise and include delayed bone healing, premature osteoarthritis, infection, nonunion, and loosening of the screw.[3] Early detection of these potential postoperative complications is important and poses a frequent radiological question in patients with postoperative pain, insufficient clinical outcome, or recurrent symptoms.

Besides conventional radiography, multidetector computed tomography (MDCT) is a commonly used imaging modality in the follow-up of scaphoid bone screw fixations.[4,5] Advantages of MDCT include high spatial resolution, robustness and wide availability.[6] The metallic hardware, however, causes beam hardening of the x-ray, typically leading to dark bands on MDCT images (referred to as streak artifacts).[7] Metal-induced artifacts often impede clear depiction of the fixation screw itself, screw bone interface (SBI), tissue in close vicinity to the implants, fracture line (FL), and consequently, the area where scaphoid bone healing takes place. To reduce streak artifacts, previous research on MDCT has focused mainly on improving scanner hardware, acquisition, and/or reconstruction parameters.[7–11]

An alternative imaging approach uses volume imaging with active matrix flat-panel detectors and cone-beam geometry, as opposed to the traditional detector design and fan-beam geometry of MDCT. This technique may show fewer artifacts, reduced radiation dose, and higher spatial resolution compared with MDCT.[12–15] This flat-panel technology can be encountered in various designs, one of which are units that feature a flat-panel detector mounted onto a fully mobile C-arm. It is hence referred to as C-arm flat-panel computed tomography (FPCT).[12,13] These units are often used for angiographic suites and other intraoperative imaging.[12] More compact designs offer flat-panel detector technology in smaller gantries with smaller detector sizes and consecutively smaller scan field of views. These so-called cone-beam computed tomography (CBCT) scanners are frequently used for dedicated craniofacial imaging but have recently become available for imaging of the appendicular skeleton and peripheral joints, including the wrist. Cone-beam computed tomographies are frequently advertised for improved patient comfort and versatility, for example, to acquire images in supine or upright weight-bearing conditions.[16,17]

To our knowledge, there are currently no studies that have systematically and directly compared the different computed tomography (CT) modalities for the postoperative evaluation of internally fixated scaphoid bone fractures and the respective impact of metallic artifacts. Thus, the aim of this prospective study was to evaluate metal-induced artifacts from fixation screws and to compare image quality among FPCT, CBCT, and standard MDCT.

MATERIALS AND METHODS

Cadaveric Specimens

No ethical board approval was required for this ex vivo cadaver study. All specimens were from individuals who had voluntarily donated their bodies to the Institute of Anatomy of our university for research purposes. All specimens were used in accordance with institutional laws

Received for publication November 20, 2013; and accepted for publication, after revision, January 29, 2014.

From the *Institute of Diagnostic and Interventional Radiology and †Division of Plastic and Reconstructive Surgery, University Hospital Zurich; ‡Institute of Anatomy, University Zurich; and §Department of Radiology, Orthopaedic University Hospital of Balgrist, Zurich, Switzerland.

Conflicts of interest and sources of funding: No funding for this work was received from National Institutes of Health (NIH), Wellcome Trust, Howard Hughes Medical Institute (HHMI), and others.

Reprints: Roman Guggenberger, MD, Institute of Diagnostic and Interventional Radiology, University Hospital Zurich, Raemistr. 100, 8091 Zurich, Switzerland. E-mail: roman.guggenberger@usz.ch.

ISSN: 0020-9996/14/4908–0532

and regulations. In total, 6 cadaveric wrists (4 right and 2 left wrists) from 4 different individuals were used. Each specimen consisted of a hand, wrist, and distal forearm and was conserved in dedicated Thiel solution, allowing for deformable conservation of soft tissues. The donors had no history of fracture or operation of the forearm or wrist bones. The name, age, and sex of the donators were blinded to us.

Scaphoid Fixation Screws

Three different types of headless and cannulated fixation screws (MEDARTIS Corp, Basel, Switzerland; SYNTHES Corp, West Chester, PA; MARTIN Corp., Jacksonville, FL), which are widely used for internal fixation of scaphoid fractures, were included in this study.[18,19] All screws were made of a titanium alloy and measured between 20 mm (MARTIN Corp) and 26 mm (MEDARTIS Corp, SYNTHES Corp.) in screw length and 2.0 mm (MARTIN Corp), 2.2 mm (MEDARTIS Corp), and 3.0 mm (SYNTHES Corp) in leading thread diameter. These were inserted in the cadaveric scaphoid bones by 1 experienced hand surgeon (MC) to fix an artificially induced fracture through the center of the scaphoid.

Image Acquisition

Imaging of the 6 wrist specimens was performed in 45° and 90° positions of the scaphoid screws in relation to the axial scanning plane (in-plane, Fig. 1). Both screw positions are routinely used for scaphoid imaging and, for example, according Buckwalter et al,[20] the position of the screws in relation to the z-axis of the CT scanner might have an influence on the degree of the emerging metal artifacts. Scan protocols of the different modalities were selected according to vendor-specific presets for wrist imaging.

Multidetector CT was performed using a second-generation dual-source CT machine (Somatom Definition Flash, Siemens Healthcare, Forchheim, Germany) operated in single energy mode. The standard wrist protocol at our institution was used: slice acquisition, 128 × 0.6 mm; pitch, 0.8; rotation time, 0.5 seconds; tube voltage, 120 kVp; and tube current-time product, 183 mAs/rotation. Images were reconstructed with a slice thickness of 0.75 mm (increment, 0.5 mm), using a field of view (FOV) of 125 × 125 mm with an image matrix of 512 × 512, resulting in a pixel size of 200 × 200 μm (Table 1).

Flat-panel CT scans were performed on an angiographic unit (Artis Zeego multiaxis system, Siemens Medical Solutions, Forchheim, Germany) with a C-arm flat-panel detector. Flat-panel CT acquisitions were conducted with detector dimensions of 30 × 38 cm with a detector size of 154 × 154 μm. A 2 × 2 binning mode was used for volume scans, and using predefined medium size, volume-of-interest raw data were reconstructed to isotropic voxels of 290 μm edge length. Two clinically approved vendor presets differing in scan length and radiation dose (5- and 20-second protocol) were used, further referred to as FPCT low- and FPCT standard-dose acquisitions, respectively. Tube current-time product was determined automatically and ranged between 29 and 66 mAs, and a small focus size of 0.6 mm without zoom factor was used (Table 1).

Cone-beam CT acquisitions were acquired on a mobile CT machine (Planmed Verity; Planmed Oy, Helsinki, Finland) using 2 standard imaging protocols with a low and standard radiation dose in analogy to FPCT (low, 80 kV, 9.5 mAs; standard, 96 kV, 12 mAs). The reconstructed voxel measured 400 μm in edge length (Table 1).

Postprocessing was performed using commercially available software (Syngo, software VE40A) on a dedicated workstation (MMWP; Siemens HealthCare). Multiplanar reformations (MPRs) in the axial, sagittal, and coronal planes were generated for all 3 modalities using a high-frequency/bone kernel with standardized parameters: FOV, 125 × 125 mm; slice thickness, 1 mm; and increment, 0.5 mm. The MPR images were eventually loaded to the picture archiving and communication system of the hospital (IMPAX 5.01; AGFA Healthcare, Moertel, Belgium) for the ensuing analysis.

Image Analysis

One reader (a radiologist with 2 years of experience in musculoskeletal imaging) performed the quantitative analysis. Two radiologists (TF and FM with 2 years of experience in musculoskeletal imaging each) who were blinded to the modality and acquisition protocol performed the qualitative analysis by independent evaluation of all images in random order. Patient information and technical parameters were blinded to the readers by the study supervisor and a homogeneous appearance of images was obtained using comparable window settings.

For quantitative image analysis, region of interest (ROI) measurements were performed for all modalities on axial reformations by 1 observer 2 times with a time lag of about 3 months. To assess stability and comparability of attenuation values among modalities, mean attenuation (in Hounsfield units, HU) and noise (standard deviation of attenuation) of cartilage not affected by metal-induced artifacts were measured.[21] Therefore, circular ROIs with a defined area of 0.7 mm^2 were placed in the articular cartilage of the wrist bones. Likewise and using the same technique, streak artifacts caused by the scaphoid screws were quantified by the attenuation difference (in HU) that resulted from measurements in wrist cartilage between an area affected by the most pronounced hypodense streak

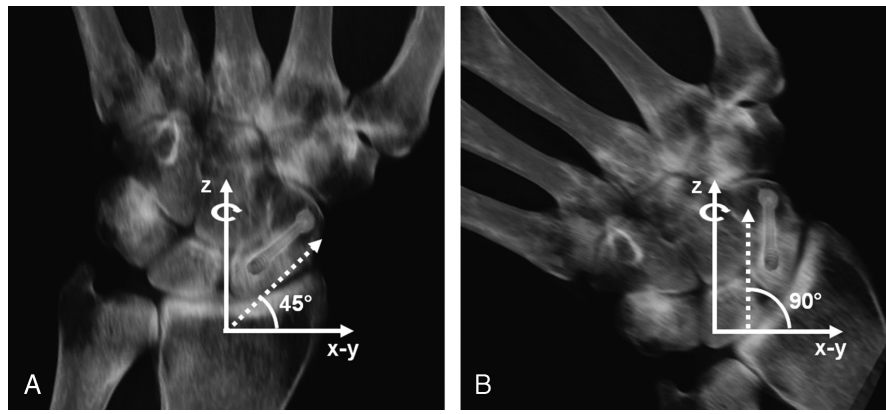

FIGURE 1. The 2 different positions of the scaphoid screw in relation to the x/y-axis (in-plane) of the scanners. The z-direction is along the longitudinal axis of the subject (through-plane) and represents the rotational axis of the gantry (curved arrow). Shown is the scaphoid screw with 45° (A) and with 90° (B) orientation in relation to the x/y-axis of the scanner (in-plane).

TABLE 1. Scan Protocols for MDCT, FPCT, and CBCT (Low and Standard Dose) Acquisitions

	MDCT	FPCT Low	FPCT Standard	CBCT Low	CBCT Standard
Tube voltage, kVp	120	70	70	80	96
Tube current-time product	183 ref mAs	Automatic: range, 29-66 mAs	Automatic: range, 29-66 mAs	9.5 mAs	12 mAs
Focal spot size, mm	0.6	0.6	0.6	0.6	0.6
Rotation angle, °	360	200	200	210	210
No. projections	–	133	496	300	300
Radiation dose	18 mGy (CTDIvol) –243 mGy × cm (DLP)	267 mGy × cm^2 (DAP)	960 mGy × cm^2 (DAP)	600 mGy × cm^2 (DAP)	1432 mGy × cm^2 (DAP)
Rotation time, s	0.5	5	20	18	18
Recon. slice thickness, mm	1	1	1	1	1
Increment	0.5	0.5	0.5	0.5	0.5
FOV, mm × mm	125 × 125	125 × 125	125 × 125	125 × 125	125 × 125
Matrix size	512 × 512	512 × 512	512 × 512	512 × 512	512 × 512

MDCT indicates multidetector computed tomography; FPCT, flat-panel computed tomography; CBCT, cone-beam computed tomography; FOV, field of view; CTDIvol, volume CT dose index; DLP, dose-length product; DAP, dose area product.

and an area not affected by streak artifacts. The absolute value of each measurement was used. This artifact-induced attenuation difference is referred to as artifact extent.

For qualitative image analysis, a bone window was chosen and manual window width/level adjustment was performed if the presetting was considered suboptimal. Both readers independently classified 4 different image quality criteria using a 5-point Likert scale (0–5)[22]: artifact degree, 0 (no artifacts/fully diagnostic) to 5 (massive artifacts/non diagnostic); FL evaluation, 0 (FL not assessable) to 5 (FL fully assessable); trabecular bone (TB) evaluation, 0 (TB not definable) to 5 (TB perfectly definable); and SBI evaluation, 0 (no SBI differentiation) to 5 (sharp SBI differentiation). Qualitative image analysis was performed on all MPR images from all modalities.

To estimate radiation doses, the volume CT dose index and dose length product (DLP) were taken from the study protocol provided by the MDCT scanner. Accordingly, the dose area product (DAP) was taken from the study protocol provided by the FPCT scanners, whereas the DAP of the CBCT scanner was specifically requested from and calculated by the vendor based on respective scanner presets.

Statistical Analysis

All calculations were conducted using commercially available software (IBM SPSS Statistics, version 20, IBM Corp., Somers, NY). Statistics were conducted by a musculoskeletal radiologist with 10 years of expertise in biomedical research. Comparisons of attenuation (HU) and noise (standard deviation of HU) of the articular cartilage tissue, artifact-induced attenuation differences, and image quality criteria (artifact degree, FL, TB, and SBI evaluation) among the 5 different acquisitions (MDCT, FPCT low, FPCT standard, CBCT low, and CBCT standard dose) were performed using related samples Friedman analyses, followed by post hoc Wilcoxon signed-rank analyses to test for paired differences. Interreader agreement for qualitative measures was analyzed by calculating Cohen κ coefficient, where 0.21 to 0.40 indicated fair; 0.41 to 0.60, moderate; 0.61 to 0.80, good; and greater than 0.81, excellent agreement.[23] Intraclass correlation coefficient was used to determine the intraobserver reliability with similar gradings of agreement as used in κ statistics. A 2-tailed P value of <0.05 was considered statistically significant.

RESULTS

A summary of the descriptive analysis for quantitative and qualitative data of both readers for all modalities is provided in Tables 2 and 3.

Quantitative Analysis

Intraobserver reliability was determined by intraclass correlation coefficient and ranged between 0.74 and 0.91, indicating good to excellent agreement (Table 4).

Mean HU values of cartilage areas not affected by artifacts showed no significant difference among modalities and dose protocols ($P = 0.07$, Fig. 2). The FPCT low-dose acquisitions had a significantly higher image noise, that is, standard deviation of cartilage attenuation, compared with all other modalities and dose protocols ($P < 0.001$, Fig. 3).

No difference in artifact extent among the different screw types for all modalities was seen ($P = 0.4$–0.9). Although higher artifact extent was seen in the 45° position, there was no significant difference to the 90° screw position in any of the 3 different modalities ($P = 0.05$–0.9, Table 5).

TABLE 2. Descriptive Quantitative Values for Different Modalities and Screw Positions

		MDCT	FPCT Low	FPCT Standard	CBCT Low	CBCT Standard
Cartilage attenuation outside artifacts, HU	45°	109 ± 38	137 ± 76	172 ± 50	142 ± 83	160 ± 63
	90°	133 ± 17	152 ± 49	154 ± 39	206 ± 70	210 ± 45
Cartilage attenuation inside artifacts, HU	45°	161 ± 40	46 ± 13	211 ± 53	246 ± 118	211 ± 53
	90°	113 ± 28	52 ± 19	153 ± 60	316 ± 78	355 ± 68

45° and 90° positions refer to the orientation of the screw in relation to the x/y-axis of the scanner. Data are presented as mean ± SD.

MDCT indicates multidetector computed tomography; FPCT, flat-panel computed tomography; CBCT, cone-beam computed tomography; HU, Hounsfield units measured inside and outside an area of the most pronounced hypodense streak.

TABLE 3. Descriptive Qualitative Values and Interreader Agreements (Cohen κ) for Both Readers

	Reader 1					Reader 2					
	MDCT	FPCT Low	FPCT Standard	CBCT Low	CBCT Standard	MDCT	FPCT Low	FPCT Standard	CBCT Low	CBCT Standard	κ
Artifact degree	1.1 ± 0.3	2.9 ± 0.3	1.7 ± 0.5	2.8 ± 0.4	2.1 ± 0.7	1.1 ± 0.3	2.8 ± 0.4	1.7 ± 0.5	2.8 ± 0.5	2 ± 0.6	0.77
Fracture line	3.7 ± 0.7	2.6 ± 0.5	3.9 ± 0.5	2.9 ± 0.5	3.4 ± 0.5	4.1 ± 0.3	2.7 ± 0.5	3.8 ± 0.6	2.8 ± 0.4	3.4 ± 0.5	0.76
Trabecula evaluation	4.2 ± 0.4	2.8 ± 0.5	4.1 ± 0.5	3.2 ± 0.6	3.5 ± 0.5	4.3 ± 0.5	2.8 ± 0.5	4 ± 0.6	3.4 ± 0.7	3.7 ± 0.5	0.76
Screw bone interface	3.8 ± 0.6	3.4 ± 0.8	4.2 ± 0.4	2.6 ± 0.5	3.4 ± 0.5	4 ± 0.4	3.3 ± 0.8	4 ± 0.6	2.8 ± 0.6	3.5 ± 0.5	0.78

Data are presented as mean ± SD.

MDCT indicates multidetector computed tomography; FPCT, flat-panel computed tomography; CBCT, cone-beam computed tomography.

Overall, significant differences among the 5 different scan protocols were seen for all measurements of artifact extent ($P < 0.001$). In MDCT and FPCT standard-dose acquisitions, the measured artifact extent was significantly smaller compared with that in the CBCT low- and standard-dose acquisitions (all $P < 0.05$, Fig. 4). No significant difference in artifact extent was noted between MDCT and FPCT standard-dose ($P = 0.48$) and between low- and standard-dose acquisitions in FPCT ($P = 0.81$) and CBCT ($P = 0.64$).

Qualitative Analysis

Cohen κ ranged between 0.76 and 0.78 and showed good agreement between both readers for the different qualitative parameters (Table 3).

Multidetector CT showed significantly lower ratings for metal-induced artifacts than all other modalities and dose protocols ($P < 0.001$). The FPCT standard-dose protocol showed lower ratings for metal-induced artifacts compared with FPCT low- and CBCT low- and standard-dose acquisitions (all $P < 0.05$). Both the MDCT and FPCT standard-dose protocols showed equal ratings for SBI, FL, and TB evaluation ($P = 0.06$, 0.2, and 0.2, respectively) and performed significantly better than FPCT low- and CBCT low- and standard-dose acquisitions (all $P < 0.05$). In general, the FPCT and CBCT standard-dose protocols performed better than respective low-dose acquisitions (all $P < 0.05$). Interestingly, there was no significant difference between FPCT low-dose and CBCT high-dose acquisitions with regard to depiction of SBI ($P = 0.6$). Artifact degree and visibility of FL were equally rated in the FPCT and CBCT low-dose acquisitions ($P = 0.4$ and 0.058) (Figs. 5 and 6).

Radiation Dose Estimations

The radiation dose of each modality and protocol is provided in Table 1. For MDCT, the volume CT dose index was 18 mGy and the DLP was 243 mGy × cm. The low-dose CBCT protocol had a DAP of 600 mGy × cm^2, which was 2.2 times higher than the DAP of the low-dose FPCT protocol (267 mGy × cm^2). The standard-dose CBCT protocol had a DAP of 1432 mGy × cm^2, which was 1.5 times higher than the DAP of the standard-dose FPCT protocol (960 mGy × cm^2).

DISCUSSION

Metal-induced artifacts often impede clear depiction of the fixation screw itself and the area near where bone healing takes place. This hampers the early detection of potential postoperative complications. Hence, the aim of this study was to evaluate metal-induced artifacts from fixation screws and to compare image quality among MDCT, FPCT, and CBCT.

However, alternative CT imaging systems using flat-panel detectors and cone-beam geometry have gained much interest in the past few years as these systems may show fewer artifacts, allow reduction of radiation dose, and provide higher spatial resolution.[12–15]

Because of inherent fundamental physical differences between the different CT modalities, several issues arise and hamper a systematic comparison. First, imaging protocols, resolution, and consecutively, image noise are usually different. For this study, we used vendor-recommended low- and standard-dose protocols for CBCT and FPCT and attempted to closely match the reconstruction processes of raw data (ie, reconstruction FOV, slice thickness, and increment) between different modalities. Another critical issue is the stability of attenuation values, which may vary between and within different scanners. Computed tomography values may be inadequately normalized for the usual scale, which sets air at 1000 HU and water at 0 HU.[24] We estimated the stability of the attenuation values by comparing the mean articular cartilage attenuation outside an area affected by artifacts and found no significant difference among the 3 modalities. This finding strongly suggests adequate calibration and, thus, comparability of measured attenuation values and artifact-induced attenuation changes in this study. However, the standard deviation for cartilage attenuation of the FPCT low-dose acquisition was significantly greater compared with that of the other acquisitions and modalities. This was likely caused by the substantially lower number of projections and, consequently, much smaller radiation dose of the FPCT low acquisitions.

TABLE 4. Intraobserver Reliability for Artifact Extent Measurements

	MDCT	FPCT Low	FPCT Standard	CBCT Low	CBCT Standard	All
ICC outside artifacts	0.89	0.91	0.84	0.86	0.73	0.78
ICC inside artifacts	0.77	0.85	0.82	0.81	0.74	0.77
P	<0.05	<0.05	<0.05	<0.05	<0.05	<0.05

For ICC outside/inside artifacts, ICC was used to determine the intraobserver reliability for region of interest measurements in wrist cartilage outside and inside metal artifacts at a time lag of about 3 months for the different modalities and protocols.

MDCT indicates multidetector computed tomography; FPCT, flat-panel computed tomography; CBCT, cone-beam computed tomography; ICC, intraclass correlation coefficient.

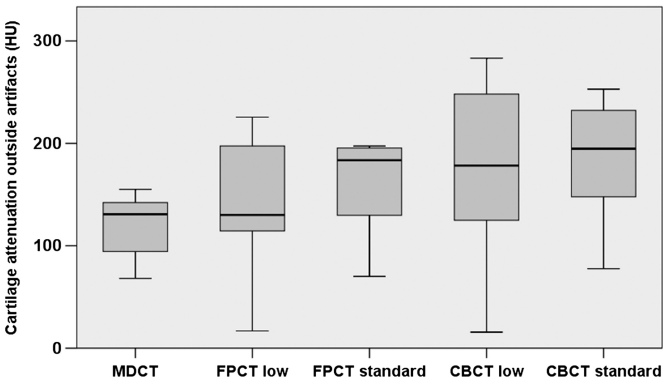

FIGURE 2. Comparison of the attenuation (in HU) measured in an articular cartilage area of the wrist outside metal artifacts between the different modalities and dose protocols. Mean HU values of cartilage areas not affected by artifacts showed no significant difference among modalities and dose protocols, suggesting adequate calibration and, thus, comparability of measured attenuation values and artifact induced attenuation changes in this study.

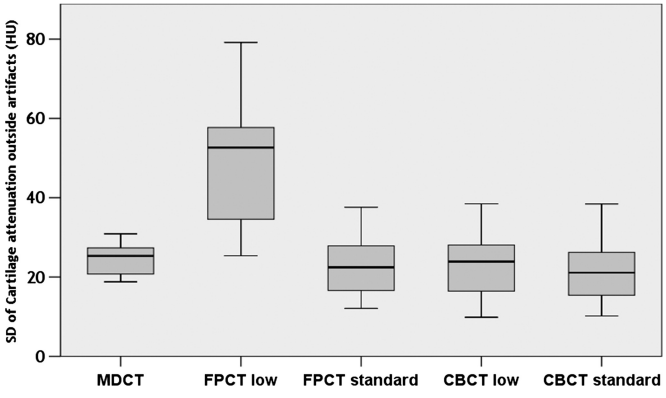

FIGURE 3. Comparison of the standard deviation of attenuation measured in an articular cartilage area of the wrist outside metal artifacts between the different modalities and dose protocols. The standard deviation for cartilage attenuation of the FPCT low acquisition was significantly higher compared with that of other modalities and dose protocols.

Scan time for MDCT lasts only about 0.5 to 2 seconds and is therefore less prone to movement artifacts, whereas FPCT and CBCT acquisitions usually take between 5 and 20 seconds. In addition, potential patient movements are more likely to affect only parts of the MDCT spiral acquisitions, whereas the entire volume dataset of FPCT and CBCT is impaired because of the use of flat-panel detectors. However, movement artifacts in imaging of peripheral appendicular structures are not very frequent and usually not as severe as in craniofacial, chest, or abdominal imaging.[15]

No difference in the artifact-induced attenuation changes among different screw types for the 3 modalities was seen. In the past, internal fixation screws widely differed in construction design and alloy composition (ie, stainless steel or titanium), leading to marked variances of artifacts.[25] The screws used in this study are current products from the major vendors.[18,19] Despite some minor differences in length and diameters, all are made of titanium alloy with similar shapes (ie, headless and cannulated), minimizing the differences in artifact. Scanning position of the scaphoid screws (ie, 45° vs 90° in relation to x/y-axis of the scanner) had no significant influence on quantitative artifact degree and image quality criteria. Similar to other studies,[26] our investigations showed a trend, but without statistical significance, for MDCT to have more prominent artifacts with transverse orientation of the scaphoid screw (ie, 45°) versus parallel orientation along the z-axis of the scanner (ie, 90°).

The current literature reflects conflicting opinions regarding metal-induced artifacts in CBCT. Some studies postulate that CBCT causes less metal streak artifacts than MDCT does[15,27] because of its favorable depiction of high-contrast structures. However, CBCT may show other and more artifacts, which are commonly unknown from MDCT, such as aliasing caused by cone-beam divergence, scatter, and a higher noise level as an important image deteriorating factor.[14,15] This is supported by our finding where both CBCT low- and standard-dose acquisitions showed significantly higher metal-induced artifact extent than the MDCT and FPCT standard-dose acquisitions did, whereas the latter 2 showed similar artifact extent. In addition, MDCT and FPCT standard-dose acquisitions had lower qualitative ratings for artifact degree and higher ratings for SBI, FL, and TB evaluation than CBCT low- and standard-dose acquisitions did.

It is known that, because of their intrinsic higher resolution, flat-panel detectors reveal the TB network very well and allow depiction of bone architecture almost on a microscopic level.[12,28,29] Our findings support this observation as the qualitative ratings for FPCT standard-dose acquisitions for TB evaluation were among the highest of all modalities in our study. In addition, SBI and FL could be equally well visualized when compared with MDCT. Metal-induced artifacts were qualitatively rated lowest for MDCT compared with all other modalities and dose protocols, even with FPCT standard. This reflects our clinical experience from daily routine where MDCT is the modality of choice in the evaluation of postoperative patients with internal fixated scaphoid bone fractures when imaging other than conventional radiography is required.[30,31] However, with the exception of qualitative ratings for artifact degree, FPCT standard-dose acquisitions performed equal to MDCT. Used intraoperatively, FPCT mounted onto a fully mobile C-arm may therefore offer sufficient image quality to adequately ascertain screw position and fracture fragment adaption. With recent metal artifact reduction algorithms on the rise[32] and in view of these study findings, the performance of flat-panel detector CTs may further increase in the near

TABLE 5. Artifact-Induced Mean Absolute HU Differences (= artifact extent) in Articular Cartilage for the 45° and 90° Screw Scanning Positions

	MDCT	FPCT Low	FPCT Standard	CBCT Low	CBCT Standard
45° position	63 ± 40	104 ± 142	53 ± 22	113 ± 91	140 ± 96
90° position	26 ± 12	51 ± 25	48 ± 50	129 ± 64	145 ± 94
P	0.05	0.38	0.82	0.73	0.94

45° and 90° positions refer to the orientation of the screw in relation to the x/y-axis of the scanner. Data are presented as mean ± SD.

HU indicates Hounsfield units; MDCT, multidetector computed tomography; FPCT, flat-panel computed tomography; CBCT, cone-beam computed tomography.

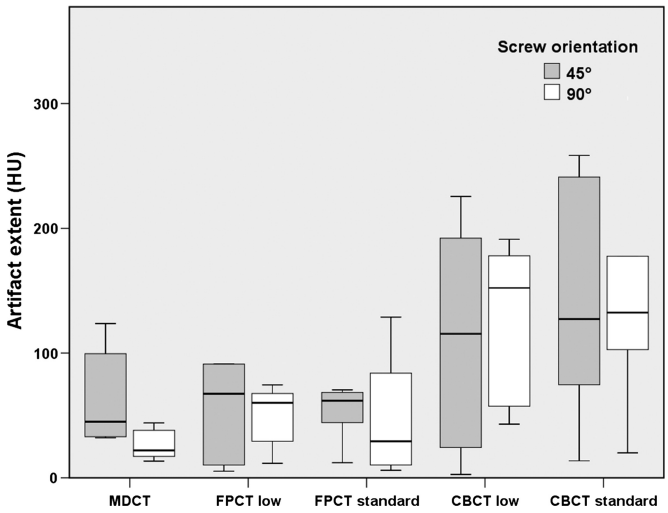

FIGURE 4. Comparison of artifact-induced attenuation differences (= artifact extent) in articular cartilage of the wrist measured in the 45° and 90° positions of the scaphoid screw in the different modalities dose protocols.

future and become a realistic alternative to MDCT imaging with a wider versatility determined by its design.

Valid radiation dose comparisons of MDCT, FPCT, and CBCT are not trivial. It is generally believed that FPCT has potentially lower radiation dose than traditional MDCT detectors do.[12,28,29] However, Kalender et al[13] state that there is no consensus at present how to compare radiation dose between modern FPCT or CBCT and traditional MDCT systems. Hence, for imaging of appendicular structures such as wrists, there is no reasonable conversion factor between DLP and DAP that would allow radiation dose comparisons between MDCT and FPCT/CBCT. As it is difficult to equalize radiation dose between modalities beforehand, we decided to use vendor-specific protocols to best approximate the routine use of the modalities used. Interestingly, both low- and standard-dose CBCT protocols had a distinctly higher DAP than the corresponding FPCT protocols.

Our study has several limitations. First, results were obtained in ex vivo experiments; however, tissue properties were preserved with dedicated Thiel solution to optimally imitate in vivo conditions. Second, even with readers blinded to the modality and acquisition protocol, the characteristic image impression of each modality might provide a bias. Third, we have not assessed dedicated metal artifact reduction algorithms. This may be an interesting topic in the near future as specific algorithms in FPCT will also allow to reduce metal artifacts and further improve orthopedic hardware imaging. Last, as

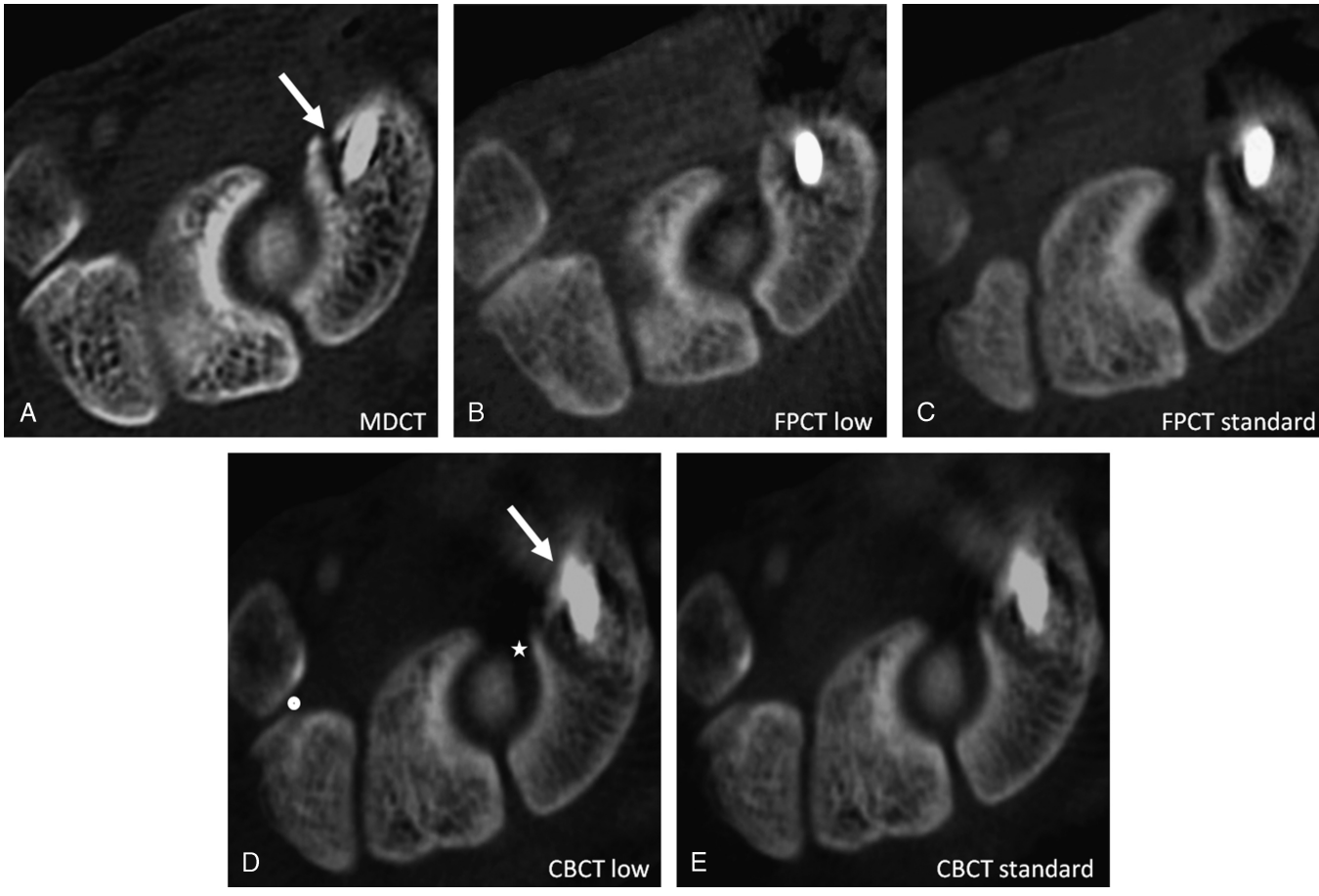

FIGURE 5. Representative example for MDCT (A) showing a well-assessable FL near the scaphoid fixation screw (arrow). MDCT (A) and FPCT standard (C) show markedly less artifacts than do CBCT low (D) and standard (E) dose acquisitions. FPCT low (B) and both CBCT acquisitions (D, E) demonstrate moderate SBI visualization, with the worst ratings for CBCT low (arrow in D). Panel D also illustrates the quantitative assessment of artifact extent, whereby an attenuation measurement is conducted by using an ROI in articular cartilage between wrist bones affected (asterisks) and not affected (dot) by metal-induced streak artifacts.

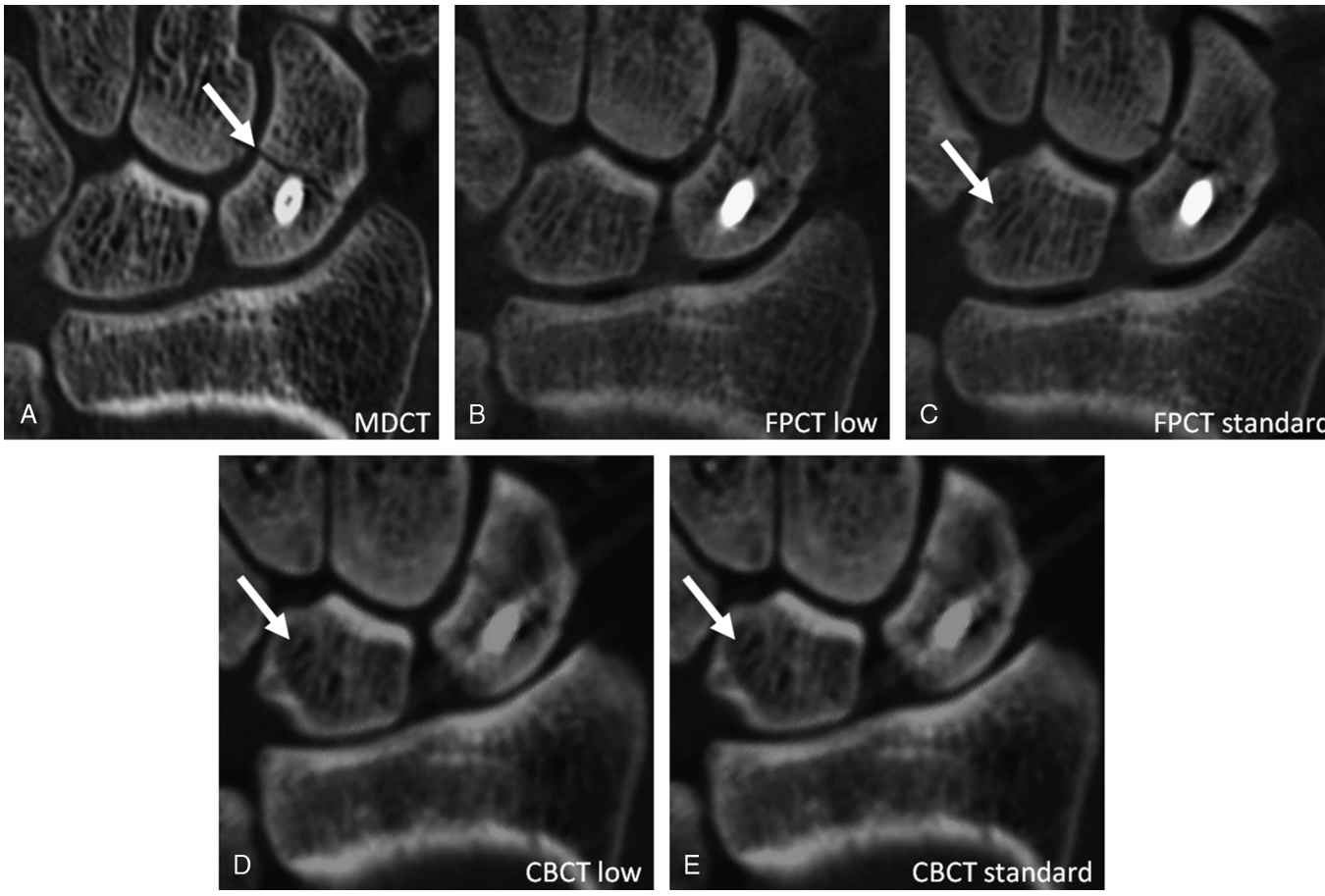

FIGURE 6. A, Sharp SBI and a fully assessable FL (arrow) for MDCT. In Panel C, FPCT standard demonstrates slightly better definable TB structure, for example, of the lunate bone (arrow), compared with FPCT low dose (B) and more clearly compared with both CBCT acquisitions (arrows in D, E). Panels D and E illustrate substantially greater metal-induced streak artifacts for CBCT in comparison with MDCT (A).

discussed earlier, although we attempted to optimally standardize protocols between modalities including acquisition and reconstruction parameters, inherent physical differences in design and beam geometry hamper systematic comparability of artifact degree and image quality. Differences in spatial resolution may be counterbalanced by differences in radiation dose, which was not harmonized between different protocols. We attempted to compare vendor-specific presets of the different modalities because a thorough balanced radiation dose between modalities is complicated and lies beyond the scope of this study. However, future studies should aim at investigating protocols using equal radiation dose and evaluating diagnostic performance in vivo.

In conclusion, MDCT and FPCT standard-dose acquisitions both showed comparatively less metal-induced artifacts and better overall image quality compared with FPCT low-dose and both CBCT acquisitions. Flat-panel CT may provide sufficient image quality to serve as a versatile CT alternative for appendicular bone imaging, particularly in view of potential future technological improvements.

ACKNOWLEDGMENTS

The authors thank Prof Dr Thomas Pfammatter (Head of Interventional Radiology, Department of Radiology, University Hospital Zurich) and Kurt Hofmann (employee of Siemens AG Healthcare Sector, Switzerland) for their advice and support during the scan acquisitions.

REFERENCES

1. Slade JF 3rd, Jaskwhich D. Percutaneous fixation of scaphoid fractures. *Hand Clin*. 2001;17:553–574.
2. Sendher R, Ladd AL. The scaphoid. *Orthop Clin North Am*. 2013;44:107–120.
3. Gutow AP. Percutaneous fixation of scaphoid fractures. *J Am Acad Orthop Surg*. 2007;15:474–485.
4. Temple CL, Ross DC, Bennett JD, et al. Comparison of sagittal computed tomography and plain film radiography in a scaphoid fracture model. *J Hand Surg*. 2005;30:534–542.
5. Lozano-Calderon S, Blazar P, Zurakowski D, et al. Diagnosis of scaphoid fracture displacement with radiography and computed tomography. *J Bone Joint Surg Am*. 2006;88:2695–2703.
6. Smith M, Bain GI, Turner PC, et al. Review of imaging of scaphoid fractures. *ANZ J Surg*. 2010;80:82–90.
7. Barrett JF, Keat N. Artifacts in CT: recognition and avoidance. *Radiographics*. 2004;24:1679–1691.
8. Kachelriess M, Watzke O, Kalender WA. Generalized multi-dimensional adaptive filtering for conventional and spiral single-slice, multi-slice, and cone-beam CT. *Med Phys*. 2001;28:475–490.
9. Veldkamp WJ, Joemai RM, van der Molen AJ, et al. Development and validation of segmentation and interpolation techniques in sinograms for metal artifact suppression in CT. *Med Phys*. 2010;37:620–628.
10. Morsbach F, Bickelhaupt S, Wanner GA, et al. Reduction of metal artifacts from hip prostheses on CT images of the pelvis: value of iterative reconstructions. *Radiology*. 2013;268:237–244.
11. Guggenberger R, Winklhofer S, Osterhoff G, et al. Metallic artefact reduction with monoenergetic dual-energy CT: systematic ex vivo evaluation of posterior spinal fusion implants from various vendors and different spine levels. *Eur Radiol*. 2012;22:2357–2364.
12. Gupta R, Cheung AC, Bartling SH, et al. Flat-panel volume CT: fundamental principles, technology, and applications. *Radiographics*. 2008;28:2009–2022.

13. Kalender WA, Kyriakou Y. Flat-detector computed tomography (FD-CT). *Eur Radiol*. 2007;17:2767–2779.
14. Schulze R, Heil U, Gross D, et al. Artefacts in CBCT: a review. *Dentomaxillofac Radiol*. 2011;40:265–273.
15. Holberg C, Steinhauser S, Geis P, et al. Cone-beam computed tomography in orthodontics: benefits and limitations. *J Orofacial Orthop*. 2005;66:434–444.
16. Tuominen EK, Kankare J, Koskinen SK, et al. Weight-bearing CT imaging of the lower extremity. *AJR Am J Roentgenol*. 2013;200:146–148.
17. Scarfe WC, Levin MD, Gane D, et al. Use of cone beam computed tomography in endodontics. *Int J Dent*. 2009;2009:634567.
18. Fowler JR, Ilyas AM. Headless compression screw fixation of scaphoid fractures. *Hand Clin*. 2010;26:351–361.
19. Grewal R, Assini J, Sauder D, et al. A comparison of two headless compression screws for operative treatment of scaphoid fractures. *J Orthop Surg Res*. 2011;6:27.
20. Buckwalter KA, Lin C, Ford JM. Managing postoperative artifacts on computed tomography and magnetic resonance imaging. *Semin Musculoskelet Radiol*. 2011;15(4):309–319.
21. Schindera ST, Diedrichsen L, Muller HC, et al. Iterative reconstruction algorithm for abdominal multidetector CT at different tube voltages: assessment of diagnostic accuracy, image quality, and radiation dose in a phantom study. *Radiology*. 2011;260:454–462.
22. Norman G. Likert scales, levels of measurement and the "laws" of statistics. *Adv Health Sci Educ*. 2010;15:625–632.
23. Viera AJ, Garrett JM. Understanding interobserver agreement: the kappa statistic. *Fam Med*. 2005;37:360–363.
24. Kyriakou Y, Kolditz D, Langner O, et al. Digital volume tomography (DVT) and multislice spiral CT (MSCT): an objective examination of dose and image quality. *RoFo*. 2011;183:144–153.
25. Sim E, Zechner W. Computerized tomography after surgical management of scaphoid fractures and pseudarthroses with implants in place. Method and results in 15 cases. *Handchir Mikrochir Plast Chir*. 1991;23:67–73.
26. Kataoka ML, Hochman MG, Rodriguez EK, et al. A review of factors that affect artifact from metallic hardware on multi-row detector computed tomography. *Curr Probl Diagn Radiol*. 2010;39:125–136.
27. Stuehmer C, Essig H, Bormann KH, et al. Cone beam CT imaging of airgun injuries to the craniomaxillofacial region. *Int J Oral Maxillofac Surg*. 2008;37:903–906.
28. Walsh CJ, Phan CM, Misra M, et al. Women with anorexia nervosa: finite element and trabecular structure analysis by using flat-panel volume CT. *Radiology*. 2010;257:167–174.
29. Reichardt B, Sarwar A, Bartling SH, et al. Musculoskeletal applications of flat-panel volume CT. *Skelet Radiol*. 2008;37:1069–1076.
30. Hackney LA, Dodds SD. Assessment of scaphoid fracture healing. *Curr Rev Musculoskelet Med*. 2011;4:16–22.
31. Dias JJ. Definition of union after acute fracture and surgery for fracture nonunion of the scaphoid. *J Hand Surg Br*. 2001;26:321–325.
32. Prell D, Kalender WA, Kyriakou Y. Development, implementation and evaluation of a dedicated metal artefact reduction method for interventional flat-detector CT. *Br J Radiol*. 2010;83:1052–1062.

